

www.acsami.org Research Article

Separation of Light Gases from Xenon over Porous Organic Cage Membranes

Jolie M. Lucero and Moises A. Carreon*



Cite This: ACS Appl. Mater. Interfaces 2020, 12, 32182-32188



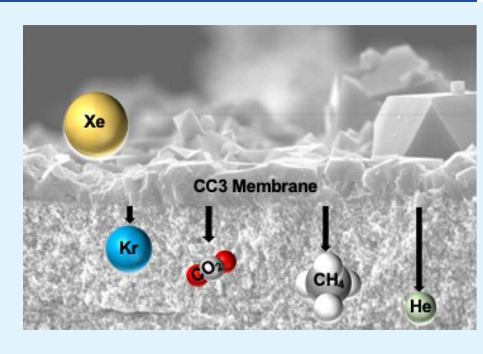
ACCESS

III Metrics & More



Supporting Information

ABSTRACT: Herein, we demonstrate the successful synthesis and separation ability of CC3 porous organic cage membranes grown on tubular supports for light gases He, CO₂, CH₄, and Kr over xenon. CC3 membranes were synthesized using secondary seeded growth and displayed different separation performances depending on the crystal size, size distribution of the seeds, and membrane thickness. CC3 membranes as thin as ~2.5 μ m resulted in high single gas permeances of 2114, 1962, 1705, 773, and 162 GPU, for He, CH₄, CO₂, Kr, and Xe, respectively. The highest ideal selectivities for He/Xe, CH₄/Xe, CO₂/Xe, and Kr/Xe gas pairs were 13, 12, 10.5, and 4.8, respectively. Mechanistically, the membranes separated He, CO₂, Kr, and CH₄ from Xe mainly via gas diffusivity differences. Therefore, the separation was kinetically driven.



KEYWORDS: membranes, porous organic cages, gas separations, xenon, light gases

1. INTRODUCTION

Chemical separations account for about 50% of the US industrial energy use and up to 15% of the US total energy consumption. Most of these industrially employed separations, including distillation, evaporation, and drying, are thermally driven. Separation technologies that do not use heat could make these separations more energy efficient. In this respect, non-thermally driven membrane technology could play a key role in making gas separations less energy intensive and therefore potentially economically feasible. When prepared in membrane form, porous crystals with uniform micropores are highly appealing materials for diverse industrially relevant gas separations. ²

In particular, porous organic cages (POCs)^{3,4} have emerged as a novel type of crystalline microporous material, which combine highly desirable properties, such as uniform micropores, high surface areas, and thermal and chemical stability, making them highly appealing candidates for diverse functional applications, including molecular gas separations. The unique structure of POCs and their distinctive solid-state molecular packing clearly differentiate them from other conventional porous materials, such as zeolites, metal organic frameworks, porous polymers, and carbon molecular sieves.^{3–8} POCs consist of covalently bonded organic cages that can assemble into crystalline microporous materials displaying three-dimensional connectivity and uniform pore size.^{3,4} Typically, these POCs are synthesized via [4 + 6] cycloimination reactions. Depending on the amine and trialdehyde employed, different cages can be formed. CC3 is the most studied prototypical type of POC.³⁻⁸ CC3 is formed by the coordination of 1,3,5triformylbenzene with trans-1,2-diaminocyclohexane, forming a porous crystalline structure with an unimodal limiting pore size of \sim 3.6 Å. Inspired by Cooper's seminal work on POCs, recently our group has demonstrated the successful synthesis of CC3 crystals via traditional solvothermal, ^{9,10} microwave, ¹¹ and evaporation-induced approaches. ¹²

Among other functional applications, CC3 has been used as the membrane for evaluating single gas permeation for several gases,⁵ separation of rare gases, including Xe and Kr,⁶ sulfur hexafluoride separation, separation of mesitylene from 4-ethyl toluene, 13 and gas chromatography separations involving chiral alcohols, ¹⁴ as the proton conductor, ¹⁵ and as a noble metal catalytic support. 16 Even if a POC phase displaying unique and remarkable separation properties is prepared in powder or particle form, the same material may be not suitable for membrane preparation due to limited adhesion of the membrane to the support, causing membrane delamination, induced stresses developed at the membrane-support interface, and/or poor crystal intergrowth, leading to discontinuous membranes. Therefore, the preparation of continuous POC membranes for molecular gas separations is not a trivial issue. Cooper's group illustrated the feasibility of synthesizing CC3 membranes on planar porous supports.

Herein, we demonstrate the successful synthesis of continuous CC3 membranes grown on alumina porous

Received: May 5, 2020 Accepted: June 22, 2020 Published: June 22, 2020





tubes, a geometry that is highly amenable for potential scaleup. We evaluated the separation performance of CC3 membranes for light gases (He, CO₂, Kr, and CH₄) over xenon. CC3 was chosen as the membrane composition based on its limiting pore aperture of ~ 3.6 Å, which is highly suitable to molecular sieve He, CO2, Kr, and CH4, having kinetic diameters of ~2.6, 3.3, 3.6, and 3.8 Å, respectively, from Xe having a kinetic diameter of ~4.1 Å. Effectively separating xenon from light gases can lead to a considerable reduction in its storage cost and in potential revenue generated from its sale. For instance, once separated, Xe can be used in lighting, as high-power lamps, 17 in medical applications (e.g., imaging and anesthesia), ^{18,19} and in the semiconductor industry.²

2. EXPERIMENTAL SECTION

2.1. Seed Synthesis. CC3 seeds were prepared following previous literature studies.^{6,9} Dichloromethane (Stabilized/Certified ACS, Fisher Scientific) (3 mL) was added slowly to 100 mg of 1,3,5triformylbenzene (98%, ACROS Organics) in a vial followed by 10 μ L of trifluoroacetic acid (99%, Alfa Aesar). In another vial, 100 mg of (±)-trans-1,2-diaminocyclohexane (99%, Sigma Aldrich) was added to 3 mL of dichloromethane and made into a homogeneous solution. The diamine solution was then added to the aldehyde solution slowly and carefully to prevent mixing. The solution was allowed to react at room temperature for 60 and 120 h. A 95:5 ethanol to dichloromethane mixture was added to each sample to harvest the CC3 crystals and centrifuged. The powder was washed 2-3 times with the ethanol/dichloromethane solution and then dried at 80°C.

2.2. Preparation of Membrane Supports. Alumina asymmetric porous tubes with 0.7 cm ID and 1.1 cm OD (100 nm inner diameter pores) were purchased from Inopor Gmbh and used as supports to grow CC3 membranes. Tubes were cut into 6 cm pieces and glazed at each end to prevent gas bypass and to provide a seal for surface Orings in the permeation unit. The effective permeation area was 6.5-7.3 cm². The supports were prepared by boiling in deionized water for 30 min a total of 3 times and dried in an oven overnight at 150°C.

2.3. Preparation of CC3 Membrane Gel. For CC3 membrane synthesis, the following synthetic procedure was used. Dichloromethane (15 mL) was slowly added to 40 mg of 1,3,5triformylbenzene in a Teflon liner followed by the addition of 100 μ L of trifluoroacetic acid. A second, homogenous solution of 45 mg of (±)-trans-1,2-diaminocyclohexane in 15 mL of dichloromethane was prepared. The diamine solution was then added to the Teflon liner.

2.4. Preparation of CC3 Membranes. Two supports were seeded with the seeds prepared previously. A 20 mg portion of 60- or 120-h seeds was suspended in dichloromethane and sonicated for 5-10 min. A bare alumina support was wrapped on the outside with Teflon tape, added to this solution, and allowed to soak for 30 min. After this, the support was removed and allowed to dry in an oven at 80°C for 1 h. This procedure was repeated 3 times, and the final seeded supports were dried overnight. Once the CC3 membrane gel was prepared, these supports were removed from the oven and allowed to cool to room temperature before being added to the Teflon liner containing the membrane gel. The Teflon liner was sealed in a Parr stainless steel acid digestion autoclave and added to a Vulcan furnace set to 50°C, for 48 h for solvothermal synthesis. After 48 h, the autoclave was cooled naturally to room temperature, and the membranes were removed and washed with ethanol and allowed to dry on the benchtop overnight before being added to an oven at 150°C. The crystals left at the bottom of the Teflon liner were harvested for XRD analysis. A diagram of this process is shown in Figure S1.

This solvothermal step was performed 2-3 times to form layers. One final CC3 layer was synthesized using a solvothermal condition of 120°C for 6 h on each membrane. Table S1 summarizes the synthesis conditions for each membrane synthesized.

2.5. Characterization. Powder X-ray diffraction data for the synthesized seeds and crystals collected from membrane solutions were recorded on a Siemens Kristalloflex 810 diffractometer using CuKα1 radiation and a wavelength of 1.54059 Å. Diffractograms were collected using a voltage of 30 kV and current of 25 mA.

Scanning electron microscopy images were collected on a FESEM JEOL JSM-7000F operated at 8-20 kV. After gas permeation, membranes were broken and imaged. Both CC3 powders and membranes were gold sputter coated before imaging to prevent charging.

Single gas permeation measurements were performed in a continuous flow system, which allows for the independent control of the feed flow rate and both feed and permeate pressures. For all studied single gases, a feed flow rate of 100 SCCMs was used, with a feed pressure of 223 kPa and permeate pressure of 85 kPa.

The flux and pressure drop across the membrane was measured in order to calculate the single gas permeation through each membrane. The permeance (P_i) was calculated by dividing the single component flux (I_i) by the driving force or pressure drop (ΔP_i) . Equations are given in the Supporting Information.

3. RESULTS AND DISCUSSION

CC3 membranes were synthesized via secondary seeded growth approach. Our group has successfully employed this approach to synthesize other porous crystalline compositions in membrane form. ^{21–23} Details on CC3 membrane synthesis are described in the Supporting Information. CC3 seed crystals were first synthesized at different synthesis times of 60 and 120 h. The PXRD patterns of these crystals are shown in Figure 1a.

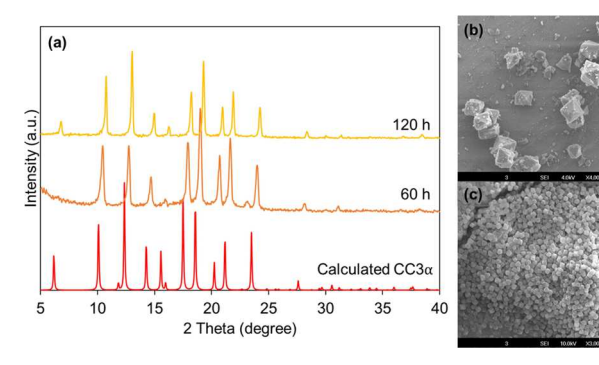


Figure 1. (a) Powder X-ray diffraction (PXRD) patterns of CC3 seeds prepared for 60 and 120 h. Representative scanning electron microscopy (SEM) images of (b) 120-h seeds and (c) 60-h seeds.

The crystalline structure of both samples corresponds to $CC3\alpha$, when comparing them to the calculated pattern. The slight peak shifts to higher 2 θ angles are characteristic of this material and suggest a contraction within cage molecules. 5

Figure 1b,c shows representative SEM images of these CC3 crystal seeds. Although both samples crystallize in the same $CC3\alpha$ phase, their morphologies are slightly different. Seed crystals synthesized for 60 h show narrow size distribution octahedral crystals in the range of 1.04 \pm 0.14 μ m, while seeds synthesized for 120 h display broader size distribution crystals with size around 3.11 \pm 1.16 μ m. The narrow size distribution and small size, make the 60-h synthesized crystals highly favorable to be used as effective seeds for membrane synthesis.²⁴ Membranes were synthesized employing these crystals as seeds via secondary seeded growth and have been denoted as M60 and M120.

Figure 2 shows representative SEM images of the synthesized CC3 membranes. Figure 2a,a' shows cross-view and top-view images respectively of the M60 membrane. This membrane is very thin, approximately 2.5 μ m. From the top

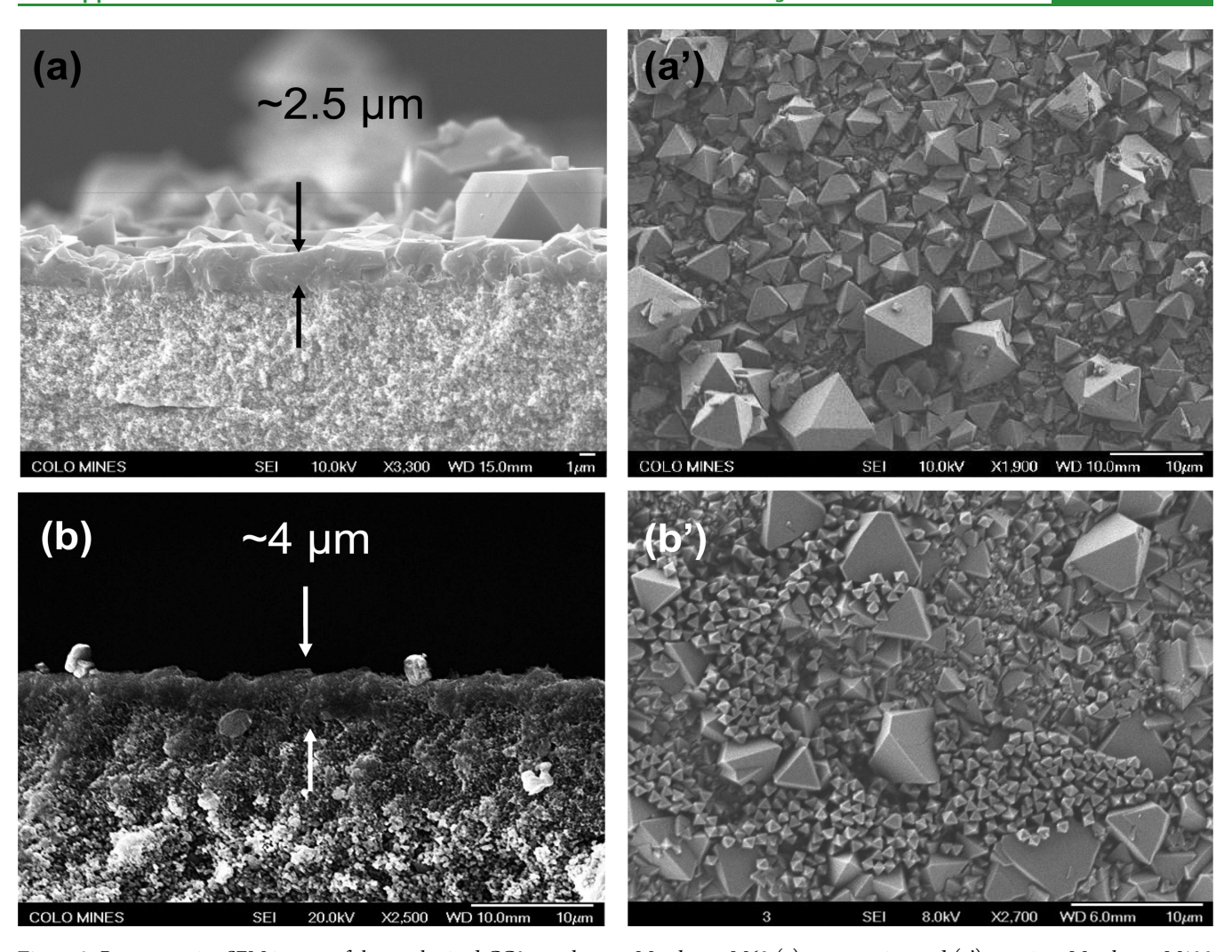


Figure 2. Representative SEM images of the synthesized CC3 membranes. Membrane M60 (a) cross-section and (a') top-view. Membrane M120 (b) cross-section and (b') top-view.

view, the membrane shows well intergrown octahedral crystals, in addition to some larger crystals. Figure 2b,b' shows representative SEM images for the membrane M120. This membrane is thicker (\sim 4 μ m) than M60. The top surface is intergrown and indicates membrane continuity but shows considerable crystal overgrowth of both large and small crystals. M120 is thicker since one additional layer was used for the synthesis of this membrane (Table S1) and also due to the fact that larger seed crystals were used to synthesize this membrane. The observed crystal size at the membrane surface was different from the original seed size, suggesting that the secondary seeded growth promoted heterogeneous nucleation at the support surface and subsequent recrystallization. Figure S2 shows PXRD patterns of CC3 crystals collected from solvothermal membrane synthesis, corresponding to a pure $CC3\alpha$ phase.

Table 1 summarizes the single gas permeances of the studied light gases through membranes M60 and M120. All gas permeances were collected using a feed pressure of 223 kPa and transmembrane pressure of 138 kPa. All gases show relatively high permeances in the \sim 162–2114 GPU range. The permeances for the studied gases through M60 were \sim 1.4–1.9 times higher than those for M120. This can be attributed to the membrane thickness increasing by about 62.5% from 2.5 up to 4 μ m for M60 and M120, respectively. In this study, we

Table 1. Single Gas Permeances and Ideal Selectivities for Light Gas *i* over Xe for CC3 Membranes

permeance[mol/m ² sPa](GPU)					
gas	M120	M60			
CH_4	3.89E-07(1162)	6.57E-07(1962)			
CO_2	2.97E-07(887)	5.71E-07(1705)			
He	4.63E-07(1382)	7.08E-07(2114)			
Kr	1.89E-07(564)	2.59E-07(773)			
Xe	8.71E-07(260) 5.44E-08(162)				
ideal selectivity					
gas pair	M120	M60			
CH ₄ /Xe	4.5	12.1			
CO ₂ /Xe	3.4	10.5			
He/Xe	He/Xe 5.3				
Kr/Xe	2.2	4.8			

focused on evaluating the separation performance of several light gases from xenon. Ideal selectivities for the following gas pairs, CH_4/Xe , CO_2/Xe , He/Xe, and Kr/Xe, are shown in Table 2. Ideal selectivities as high as 12 and 13 for CH_4/Xe and He/Xe gas pairs, respectively, were observed. Selectivities for each gas pair were about $\sim\!2.5-3$ times higher for membrane M60 than for M120. This can be possibly attributed

Table 2. Microporous Crystalline Membranes for the Separation of Light Gases from Xenon

gas pair (i/Xe)	membrane material	permeance of i (GPU)	selectivity (i/Xe)	reference
Kr/Xe	AlPO-18	940	6.4	30
Kr/Xe	ZIF-8	44	14.2	31
Kr/Xe	SAPO-34	537	45	23
Kr/Xe	SAPO-34	26	20	32
Kr/Xe	SAPO-34	12	27.5	33
Kr/Xe	CC3	773	4.8	this work
N_2/Xe	ZIF-8	117	12.4	27
N_2/Xe	SAPO-34	686	30.1	28
CO ₂ /Xe	DD3R	83	67	29
CO ₂ /Xe	CC3	1705	10.5	this work
CH ₄ /Xe	CC3	1962	12.1	this work
He/Xe	CC3	2114	13	this work

to the crystal size and size distribution of the seeds employed during secondary seeded growth. The small 60-h synthesized seeds have a narrow size distribution, and when membrane seeding takes place, these smaller crystals are able to effectively create a tightly packed seed layer on the surface of the alumina support. When solvothermal synthesis is performed, the use of smaller, and more uniform seeds, allows for a better crystal intergrowth, leading to a more uniform membrane growth. This phenomenon is well known, especially for zeolite membranes. For instance, Carreon et al. demonstrated that CO₂/CH₄ separation selectivity can be greatly improved when seed crystal size is considerably reduced.²⁴ Alternatively, when larger crystals are used for seeding, the coverage of the alumina support is not uniform, and after membrane growth, there is a higher chance of the formation of a higher concentration of defects. Larger seed crystals also contribute negatively to the formation of thicker membranes. The higher observed permeances for the studied light gases over xenon may be associated with the thinner nature of the membranes. In addition, the presence of defects (non-selective pore pathways) could potentially contribute to these high permeances. While much higher ideal separation selectivities were expected due to the CC3 limiting pore size aperture of ~3.6 Å lying between the kinetic diameters of the studied gas pairs (He, 2.6 Å; CO₂, 3.3 Å; Kr, Å; 3.6; CH₄,3.8 Å; vs Xe, 4.1 Å), it is clear that the well-known flexibility of the CC3 cage9 and the presence of defects may have limited this potential sharp molecular sieving

Figure 3 illustrates a general schematic comparing the potential effect of seed crystal size and size distribution on the formation of CC3 membranes. The definition of high quality vs highly defective has been based on the actual performance (ideal selectivities) of these two membranes.

Figure 4 illustrates light gas ideal separation selectivity over Xe as a function of molecular weight for M60. Helium showed the higher ideal selectivities to Xe among all the studied gas pairs. For each membrane M60 and M120, the ideal separation selectivity drops exponentially with an increase of molecular weight. To understand the role of diffusivity on the separation performance of the CC3 membranes, diffusion coefficients for each gas were calculated using Fick's law and are shown in Table S2.

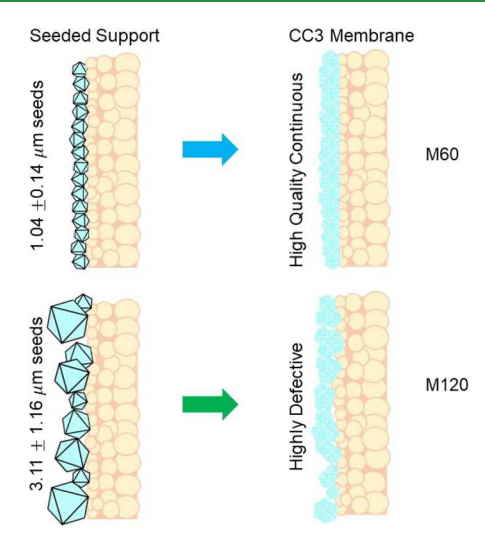


Figure 3. General schematic illustrating the quality of CC3 membranes produced from 60- and 120-h CC3 seeds.

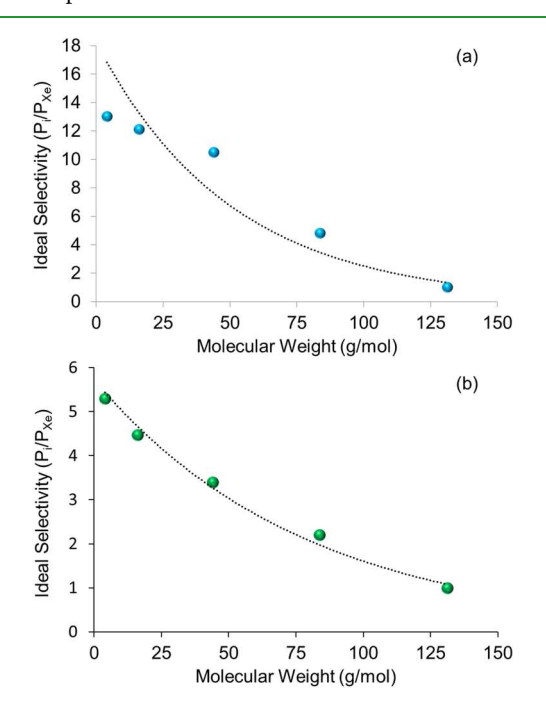


Figure 4. Ideal separation selectivity of light gas *i* over Xe as a function of molecular weight for (a) M60 and (b) M120 CC3 membranes.

The flux taken from membrane experiments, membrane thickness, and concentration gradients across the membrane were used to calculate these diffusion coefficients. For the estimation of diffusion coefficients, Ficks' law was used. The following assumptions were made: ideal gas, steady state, one-dimensioaln gas transport, and constant membrane thicknesses. All parameters were extracted from experimental data, and therefore, the calculated diffusion coefficients implicitly include adsorption effects. Helium, as expected, diffuses the fastest across both membranes with diffusivities of 4.36×10^{-9} , and 4.56×10^{-9} m²/s for M60 and M120, respectively. The studied light gases diffuse in the following order from the fastest to slowest for M120 and M60: He>CH₄>CO₂>Kr>Xe. The ideal selectivities for the separation of light gas *i* from Xe over CC3 membranes correlated linearly with the diffusivity of

gas *i*, (Figure 5) suggesting that differences in diffusivities are the main separation mechanism. M60 (blue) and M120 (green) CC3 membranes.

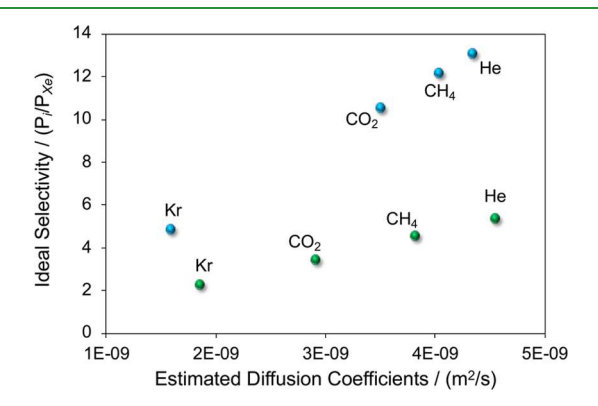


Figure 5. Ideal selectivity of gas i over Xe as a function of diffusivity coefficients for gas i.

Figure 6 shows the ideal selectivities of CC3 membranes as a function of molecule size. CC3 has a limiting pore aperture of

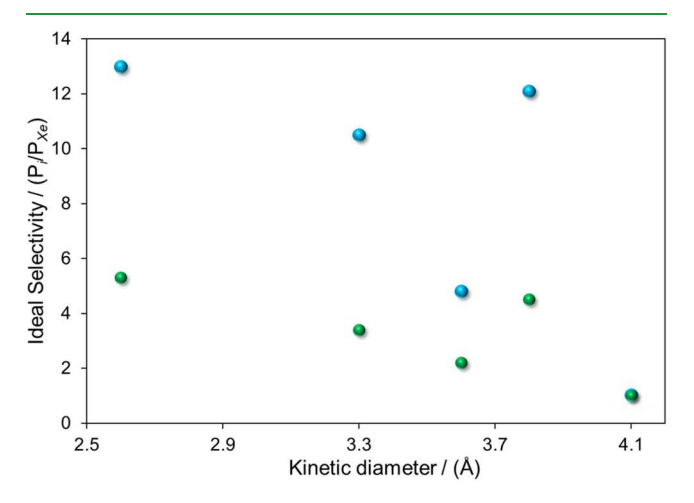


Figure 6. Ideal separation selectivity of light gas *i* over Xe with respect to the kinetic diameter of M60 (blue) and M120 (green) CC3 membranes.

3.6 Å, and therefore, molecules having a smaller size than the membrane pore size such as He and CO2 should be able to permeate through the CC3 membrane with low resistance, leading to high permeances. Therefore, differences in molecule size for He/Xe and CO₂/Xe gas pairs led to moderate ideal selectivities of 13 and 10.5, respectively. Larger gases such as Kr displayed low ideal selectivities. Kr molecule size is slightly larger or as large as the CC3 limiting window aperture, and therefore, the permeance of this molecule through CC3 is hindered (lower) as compared to CO₂ and He. Interestingly, in the case of CH₄/Xe, the moderate ideal selectivity ~12 suggests that the size of the molecule is not the key factor that leads to this observed selectivity. It is likely that the unique diamondoid pore network of CC3 can potentially impart pore shape selectivity resulting in moderate CH₄/Xe ideal selectivities. In fact, it is known that regular micropores with different geometries can potentially discriminate molecules based on their different molecular configurations.²⁵ In particular, lower hydrocarbons are known to display different

molecular configurations, leading potentially to this entropic selectivity. 25 In addition, as supported by diffusivity calculations, $\mathrm{CH_4}$ diffuses faster than all studied gas molecules (except He), a factor that should contribute positively to the observed moderate ideal selectivities.

Although in principle, molecular sieving could be possible for the studied light gases over xenon, the CC3 framework flexibility and potential disordered CC3 molecule packing²⁶ should result in the formation of non-selective pore pathways leading to a limited sieving effect. Adsorption may play an important role in the transport properties of the studied gases over CC3. Of all the studied molecules, Xe is the one having the highest isosteric heat of adsorption and highest uptake capacities over CC3 crystals.⁶ The reported isosteric heat of adsorption values in kJ/mol for He, CO₂, CH₄, Kr, and Xe are 4.8, 27.6, 22, 22.6, and 31, respectively. These values are calculated zero-coverage heats of adsorption taken from a multicomponent competitive adsorption simulation. Relative heats of adsorption ordered from the lowest to highest are He<CH₄<Kr<CO₂<Xe. These relative heats of adsorption correlate directly to the polarizability of each gas. Therefore, as compared to all studied gases, Xe will adsorb preferentially over CC3. This Xe preferential adsorption has been associated with a strong competing separation mechanism in zeolite²³ and MOF²⁷ membranes.

Table 2 summarizes the separation performance of state-ofthe-art microporous crystalline membranes for the separation of xenon from light gases. For comparison, we have included in this table the performance of our CC3 membranes for light gas separation from xenon. Note that for CC3 membranes, we report the ideal separation selectivities. By far, the most studied gas pair (for Xe separation through microporous crystalline membranes) is Kr/Xe. SAPO-34, a well-studied silico aluminophosphate membrane with a nominal pore size of 3.8 Å, exhibits the best separation performance reported for Kr/Xe mixtures, displaying a separation selectivity of Kr/Xe up to 45, with average Kr permeances as high as 537 GPU.²³ The separation is dominated by molecular sieving, as Xe (kinetic diameter = 4.1 Å) cannot effectively permeate through the zeolite pores, and diffusivity differences. Another microporous crystalline membrane denoted as AlPO-18, with a similar pore size to SAPO-34, has shown remarkably high Kr permeances.³² Both types of membranes are extremely thin (3 μ m for SAPO-34 and $\sim 2 \mu m$ for AlPO-18) and contribute to the high permeances of Kr. Recently, we documented SAPO-34 and ZIF-8 microporous crystalline membranes for the separation of air from xenon. 27,28 Again, SAPO-34 displayed the best separation performance with N₂ permeance as high as 686 GPU and N_2/Xe separation selectivities of $\sim 30.^{28}$ Recently, a small pore zeolite DD3R membrane has been reported for the separation of CO₂ from Xe.²⁹ These DDR membranes with an effective pore size of 3.6 Å display remarkably high CO₂/Xe separation selectivities up to ~67 and moderate CO₂ permeances.²⁹ Although our CC3 membranes display low to moderate ideal selectivities of diverse light gases over Xe, they exhibit one of the highest reported Kr permeances over Xe and unprecedented permeances for He, CO₂, and CH₄ over Xe. The thicknesses of our CC3 membranes are comparable to those thicknesses of high-quality SAPO-34²³ and AlPO-18³⁰ membranes.

Xenon is available in trace amounts in Earth's atmosphere and natural gas, and is produced as a byproduct when treating spent nuclear fuel. In each of these gas resources, xenon is mixed at low concentrations, with CO₂, CH₄, Kr, and He among other gases. While both parameters, separation selectivity and permeance, affect the overall economics of the separation process, the relative importance of each parameter depends on the specific application. Typically, when large amounts of gases with comparable molar ratios are separated, permeance becomes more crucial than separation selectivity. Therefore, for the studied separation, the high observed light gas permeances over xenon can potentially make these membranes highly appealing.

4. CONCLUSIONS

In summary, we have demonstrated the proof of concept on the successful development of continuous CC3 membranes grown on tubular supports displaying the ability to separate light gases from Xe at high gas permeances. The quality and integrity of the membranes were highly dependent on the crystal size and size distribution of the seeds employed for membrane synthesis. Specifically, the smaller CC3 seeds with a narrow size distribution led to membranes displaying enhanced separation performance. Mechanistically, the membranes separated He, CO2, Kr, and CH4 from Xe mainly via differences in diffusivities. Therefore, the separation was kinetically driven. The ideal separation selectivities correlated linearly with respect to gas diffusivity coefficients. While the synthesized CC3 membranes in this study displayed low to moderate ideal selectivities of the light gas over xenon (2.2-13), they displayed unprecedented high gas permeances. Specifically, He, CO₂, Kr, and CH₄ permeances of 2114, 1705, 773, and 1962 GPUs were observed. These membranes may be promising for extracting xenon from different important gas sources, including air, natural gas, medical mixtures, and nuclear-based gases. Future work will focus on assessing the performance of these membranes for gas mixtures at industrially relevant feed gas compositions, as well as on evaluating its long-term stability.

ASSOCIATED CONTENT

Supporting Information

The Supporting Information is available free of charge at https://pubs.acs.org/doi/10.1021/acsami.0c08040.

Materials and Methods, including gas permeation measurements. Diagram illustrating the CC3 membrane synthesis process. PXRD of CC3 crystals collected from membrane synthesis. Diffusion coefficients for all studied gases over CC3 membranes (PDF)

AUTHOR INFORMATION

Corresponding Author

Moises A. Carreon — Department of Chemical and Biological Engineering, Colorado School of Mines, Golden, Colorado 80401, United States; orcid.org/0000-0001-6391-2478; Email: mcarreon@mines.edu

Author

Jolie M. Lucero — Department of Chemical and Biological Engineering, Colorado School of Mines, Golden, Colorado 80401, United States; o orcid.org/0000-0002-4606-7118

Complete contact information is available at: https://pubs.acs.org/10.1021/acsami.0c08040

Notes

The authors declare no competing financial interest.

ACKNOWLEDGMENTS

M.A.C. thanks the National Science Foundation (CBET award # 1835924) for financial support.

REFERENCES

- (1) Sholl, D. S.; Lively, R. P. Seven Chemical Separations to Change the World. *Nature* **2016**, *532*, 435–437.
- (2) Carreon, M. A. Porous Crystals as Membranes. Science 2020, 367, 624.
- (3) Tozawa, T.; Jones, J. T. A.; Swamy, S. I.; Jiang, S.; Adams, D. J.; Shakespeare, S.; Clowes, R.; Bradshaw, D.; Hasell, T.; Chong, S. Y.; Tang, C.; Thompson, S.; Parker, J.; Trewin, A.; Bacsa, J.; Slawin, A. M. Z.; Steiner, A.; Cooper, A. I. Porous Organic Cages. *Nat. Mater.* **2009**, *8*, 973–978.
- (4) Jones, J. T. A.; Hasell, T.; Wu, X.; Bacsa, J.; Jelfs, K. E.; Schmidtmann, M.; Chong, S. Y.; Adams, D. J.; Trewin, A.; Schiffman, F.; Cora, F.; Slater, B.; Steiner, A.; Day, G. M.; Cooper, A. I. Modular and Predictable Assembly of Porous Organic Molecular Crystals. *Nature* **2011**, *474*, 367–371.
- (5) Song, Q. L.; Jiang, S.; Hasell, T.; Liu, M.; Sun, S. J.; Cheetham, A. K.; Sivaniah, E.; Cooper, A. I. Porous Organic Cage Thin Films and Molecular-Sieving Membranes. *Adv. Mater.* **2016**, *28*, 2629–2637.
- (6) Chen, L.; Reiss, P. S.; Chong, S. Y.; Holden, D.; Jelfs, K. E.; Hasell, T.; Little, M. A.; Kewley, A.; Briggs, M. E.; Stephenson, A.; Thomas, K. M.; Armstrong, J. A.; Bell, J.; Busto, J.; Noel, R.; Liu, J.; Strachan, D. M.; Thallapally, P. K.; Cooper, A. I. Separation of Rare Gases and Chiral Molecules by Selective Binding in Porous Organic Cages. *Nat. Mater.* **2014**, *13*, 954–960.
- (7) Hasell, T.; Miklitz, M.; Stephenson, A.; Little, M. A.; Chong, S. Y.; Clowes, R.; Chen, L. J.; Holden, D.; Tribello, G. A.; Jelfs, K. E.; Cooper, A. I. Porous Organic Cages for Sulfur Hexafluoride Separation. J. Am. Chem. Soc. 2016, 138, 1653–1659.
- (8) Liu, M.; Little, M. A.; Jelfs, K. E.; Jones, J. T. A.; Schmidtmann, M.; Chong, S. Y.; Hasell, T.; Cooper, A. I. Acid- and Base-Stable Porous Organic Cages: Shape Persistence and pH Stability via Post-synthetic "Tying" of a Flexible Amine Cage. *J. Am. Chem. Soc.* **2014**, 136, 7583–7586.
- (9) Lucero, J.; Elsaidi, S. K.; Anderson, R.; Wu, T.; Gomez-Gualdron, D. A.; Thallapally, P. K.; Carreon, M. A. Time Dependent Structural Evolution of Porous Organic Cage CC3. *Cryst. Growth Des.* **2018**, *18*, 921–927.
- (10) Lucero, J.; Osuna, C.; Crawford, J. M.; Carreon, M. A. Microwave-Assisted Synthesis of Porous Organic Cages CC3 and CC2. CrystEngComm 2019, 21, 4534–4537.
- (11) Lucero, J.; Crawford, J. M.; Osuna, C.; Carreon, M. A. Solvothermal Synthesis of Porous Organic Cage CC3 in the Presence of Dimethylformamide as Solvent. *CrystEngComm* **2019**, *21*, 5039–5044.
- (12) Lucero, J. M.; Jasinski, J. B.; Song, M.; Li, D.; Liu, L.; Liu, J.; De Yoreo, J.; Thallapally, P. K.; Carreon, M. A. Synthesis of Porous Organic Cage CC3 via Solvent Modulated Evaporation. *Inorg. Chim. Acta* 2020, 501, 119312.
- (13) Mitra, T.; Jelfs, K. E.; Schmidtmann, M.; Ahmed, A.; Chong, S. Y.; Adams, D. J.; Cooper, A. I. Molecular Shape Sorting using Molecular Organic Cages. *Nat. Chem.* **2013**, *5*, 276–281.
- (14) Kewley, A.; Stephenson, A.; Chen, L. J.; Briggs, M. E.; Hasell, T.; Cooper, A. I. Porous Organic Cages for Gas Chromatography Separations. *Chem. Mater.* **2015**, *27*, 3207–3210.
- (15) Liu, M.; Chen, L. J.; Lewis, S.; Chong, S. Y.; Little, M. A.; Hasell, T.; Aldous, I. M.; Brown, C. M.; Smith, M. W.; Morrison, C. A.; Hardwick, L. J.; Cooper, A. I. Three-Dimensional Protonic Conductivity in Porous Organic Cage Solids. *Nat. Commun.* **2016**, *7*, 12750
- (16) Sun, J. K.; Zhan, W. W.; Akita, T.; Xu, Q. Toward Homogenization of Heterogeneous Metal Nanoparticle Catalysts

- with Enhanced Catalytic Performance: Soluble Porous Organic Cage as a Stabilizer and Homogenizer. *J. Am. Chem. Soc.* **2015**, *137*, 7063–7066.
- (17) Kñfferlein, M.; Dñhring, T.; Payer, H. D.; Seidlitz, H. K. Xenon lighting adjusted to plant requirements. Tibbitts, T. W. (ed.). *International Lighting in Controlled Environments Workshop*, 1994; Vol. NASA-CP-95-3309, pp 229–242.
- (18) Bifone, A.; Song, Y. Q.; Seydoux, R.; Taylor, R. E.; Goodson, B. M.; Pietrass, T.; Budinger, T. F.; Navon, G.; Pines, A. NMR of Laser-Polarized Xenon in Human Blood. *Proc. Nat. Acad. Sci.* **1996**, 93, 12932–12936.
- (19) Holsträter, T. F. M. D.; Georgieff, M. M. D.; Föhr, K. J. P. D.; Klingler, W. M. D.; Uhl, M. E. M. D.; Walker, T. M. D.; Köster, S. P. D.; Grön, G. P. D.; Adolph, O. Intranasal Application of Xenon Reduces Opioid Requirement and Postoperative Pain in Patients Undergoing Major Abdominal Surgery: A Randomized Controlled Trial. *Anesthesiology* **2011**, *115*, 398–407.
- (20) Fujishima, A.; Honda, K. Electrochemical Photolysis of Water at a Semiconductor Electrode. *Nature* **1972**, *238*, 37–38.
- (21) Duke, M. C.; Zhu, B.; Doherty, C. M.; Hill, M. R.; Hill, A. J.; Carreon, M. A. Structural effects on SAPO-34 and ZIF-8 materials exposed to seawater solutions, and their potential as desalination membranes. *Desalination* **2016**, *377*, 128–137.
- (22) Zong, Z.; Elsaidi, S. K.; Thallapally, P. K.; Carreon, M. A. Highly Permeable AlPO-18 Membranes for N₂/CH₄ Separation. *Ind. Eng. Chem. Res.* **2017**, *56*, 4113–4118.
- (23) Feng, X.; Zong, Z.; Elsaidi, S. K.; Jasinski, J. B.; Krishna, R.; Thallapally, P. K.; Carreon, M. A. Kr/Xe Separation over a Chabazite Zeolite Membrane. *J. Am. Chem. Soc.* **2016**, *138*, 9791–9794.
- (24) Carreon, M. A.; Li, S.; Falconer, J. L.; Noble, R. D. Alumina-Supported SAPO-34 Membranes for CO2/CH4 Separation. *J. Am. Chem. Soc.* **2008**, *130*, 5412–5413.
- (25) Rungta, M.; Xu, L.; Koros, W. J. Carbon Molecular Sieve Dense Film Membranes Derived from Matrimid for Ethylene/ethane Separation. *Carbon* **2012**, *50*, 1488–1502.
- (26) Zhu, G. H.; Liu, Y.; Flores, L.; Lee, Z. R.; Jones, C. W.; Dixon, D. A.; Sholl, D. S.; Lively, R. P. Formation Mechanisms and Defect Engineering of Imine-Based Porous Organic Cages. *Chem. Mater.* **2018**, *30*, 262–272.
- (27) Wu, T.; Lucero, J.; Sinnwell, M. A.; Thallapally, P. K.; Carreon, M. A. Recovery of Xenon from Air Over ZIF-8 Membranes. *Chem. Commun.* **2018**, *54*, 8976–8979.
- (28) Wu, T.; Lucero, J.; Crawford, J. M.; Sinnwell, M. A.; Thallapally, P. K.; Carreon, M. A. SAPO-34 Membranes for Xenon Capture from Air. *J. Membr. Sci.* **2019**, *573*, 288–292.
- (29) Wang, X.; Zhang, Y.; Wang, X.; Andres-Garcia, E.; Du, P.; Giordano, L.; Wang, L.; Hong, Z.; Gu, X.; Murad, S.; Kapteijn, F. Xenon Recovery by DD3R Zeolite Membranes: Application in Anaesthetics. *Ang. Chem., Int. Ed.* **2019**, *58*, 15518–15525.
- (30) Wu, T.; Lucero, J.; Zong, Z.; Elsaidi, S. K.; Thallapally, P. K.; Carreon, M. A. Microporous Crystalline Membranes for Kr/Xe Separation: Comparison Between AlPO-18, SAPO-34, and ZIF-8. ACS Appl. Nano Mater. 2018, 1, 463–470.
- (31) Wu, T.; Feng, X.; Elsaidi, S. K.; Thallapally, P. K.; Carreon, M. A. Zeolitic Imidazolate Framework-8 (ZIF-8) Membranes for Kr/Xe Separation. *Ind. Eng. Chem. Res.* **2017**, *56*, 1682–1686.
- (32) Kwon, Y. H.; Min, B.; Yang, S.; Koh, D.-Y.; Bhave, R. R.; Nair, S. Ion-Exchanged SAPO-34 Membranes for Krypton-Xenon Separation: Control of Permeation Properties and Fabrication of Hollow Fiber Membranes. ACS Appl. Mater. Interfaces 2018, 10, 6361–6368.
- (33) Hye Kwon, Y.; Kiang, C.; Benjamin, E.; Crawford, P.; Nair, S.; Bhave, R. Krypton-Xenon Separation Properties of SAPO-34 Zeolite Materials and Membranes. *AIChE J.* **2017**, *63*, 761–769.
- (34) Koros, J.; Mahajan, R. Pushing the limits on possibilities for large scale gas separation: which strategies? *J. Membr. Sci.* **2000**, 175, 181–196.

(35) Bernardo, P.; Drioli, E.; Golemme, G. Membrane Gas Separation: A Review/State of the Art. *Ind. Eng. Chem. Res.* **2009**, 48, 4638–4663.